Biomed Microdevices (2017) 19:73
DOI 10.1007/s10544-017-0209-9

Hands-free smartphone-based diagnostics for simultaneous detection of Zika, Chikungunya, and Dengue at point-of-care

A. Ganguli[1,2] · A. Ornob[1,2] · H. Yu[2,4] · G. L. Damhorst[1,2,3] · W. Chen[2,4] · F. Sun[2,4] · A. Bhuiya[1,2] · B. T. Cunningham[1,2,4] · R. Bashir[1,2,4,5]

Abstract Infectious diseases remain the world's top contributors to death and disability, and, with recent outbreaks of Zika virus infections there has been an urgency for simple, sensitive and easily translatable point-of-care tests. Here we demonstrate a novel point-of-care platform to diagnose infectious diseases from whole blood samples. A microfluidic platform performs minimal sample processing in a user-friendly diagnostics card followed by real-time reverse-transcription loop-mediated isothermal amplification (RT-LAMP) on the same card with pre-dried primers specific to viral targets. Our point-of-care platform uses a commercial smartphone to acquire real-time images of the amplification reaction and displays a visual read-out of the assay. We apply this system to detect closely related Zika, Dengue (types 1 and 3) and Chikungunya virus infections from whole blood on the same pre-printed chip with high specificity and clinically relevant sensitivity. Limit of detection of 1.56e5 PFU/mL of Zika virus from whole blood was achieved through our platform. With the ability to quantitate the target nucleic acid, this platform can also perform point-of-care patient surveillance for pathogen load or select biomarkers in whole blood.

Keywords Loop mediated isothermal amplification · Point-of-care diagnostics · Zika diagnostics · Smartphone diagnostics · Hands-free microfluidics

1 Introduction

A member of the family *Flaviviridae*, genus *Flavivirus*, Zika virus appeared in the international spotlight in late 2015 as evidence emerged of a possible link between an epidemic affecting Brazil and increased rates of microcephaly in newborns (Kleber de Oliveira et al. 2016). Like other febrile virus infections such as Dengue and Chikungunya, Zika virus is transmitted by the bite of infected *Aedes aegypti* and *Aedes albopictus* mosquitos (Baden et al. 2016). Human-to-human spread is also well documented, including *in utero* transmission from mother to fetus, sexual transmission, and in one unusual case, non-sexual spread through close contact with an individual of high viremia, likely sweat or tears (Swaminathan et al. 2016). While most Zika virus infections are asymptomatic, those who manifest disease typically exhibit non-specific symptoms including to varying degrees: rash, fever, arthralgia, conjunctivitis, myalgia, headache, retro-orbital pain, edema, and vomiting (Lessler et al. 2016; van der Linden et al. 2016), many of which overlap significantly with acute Dengue and Chikungunya virus infections. Moreover, Zika virus infection has been reported to cause Guillain-Barré syndrome, a neurological complication

A. Ganguli and A. Ornob contributed equally to this work

Electronic supplementary material The online version of this article (doi:10.1007/s10544-017-0209-9) contains supplementary material, which is available to authorized users.

✉ B. T. Cunningham
bcunning@illinois.edu

✉ R. Bashir
rbashir@illinois.edu

[1] Department of Bioengineering, University of Illinois at Urbana-Champaign, Champaign, IL, USA

[2] Micro and Nanotechnology Laboratory, University of Illinois at Urbana-Champaign, Champaign, IL, USA

[3] College of Medicine at Urbana-Champaign, University of Illinois, Champaign, IL, USA

[4] Department of Electrical and Computer Engineering, University of Illinois at Urbana-Champaign, Champaign, IL, USA

[5] Carle Illinois College of Medicine, Urbana, IL, USA

Published online: 22 August 2017

involving progressive paralysis capable of resulting in respiratory failure and death (Lessler et al. 2016; van der Linden et al. 2016).

The non-specific presentation of Zika virus symptoms and shared vectors with other febrile diseases such as Dengue and Chikungunya present a significant diagnostic challenge: no combination of symptoms is adequately unique to make a clinical diagnosis of Zika virus. The problem is aggravated in some resource-limited regions where all the three virus infections are endemic resulting in the need for specific diagnosis for informed clinical intervention, better patient management, and epidemiological surveillance (Waggoner et al. 2016a; Waggoner et al. 2016b). This creates a need for low-cost and portable platforms that can provide fast, accurate, and multiplexed diagnosis of all such diseases at the point-of-care. The current gold standard in Zika virus detection involves nucleic acid detection (RT-PCR) and antibody serology with an immunoassay (Lessler et al. 2016). A major challenge, however, is cross-reactivity of antibodies in individuals with prior Dengue infection, rendering serology an imperfect approach that can be difficult to interpret in such scenarios (Lessler et al. 2016). RT-PCR, meanwhile, remains an expensive, highly-technical, and time-consuming method making it incompatible in regions with poor healthcare infrastructure.

Loop-mediated isothermal amplification (LAMP), emerged within the last two decades as an alternative to PCR for nucleic acid amplification (Notomi et al. 2000). This method has been leveraged for higher specificity of its 4–6 primer systems, single-temperature incubation, and increased resistance of the *Bst* polymerase to inhibitors that prevent PCR. LAMP and RT-LAMP have been employed in the literature for a variety of nucleic acid detection applications including point-of-care platforms (Damhorst et al. 2015; Duarte-Guevara et al. 2014, 2016; Notomi et al. 2015; Safavieh et al. 2016). and, in just a few recent reports, Zika virus detection (Song et al. 2016; Tian et al. 2016; Wang et al. 2016; Lee et al. 2016). Few, however, have leveraged the robustness of the LAMP polymerase for detection of pathogens directly in unprocessed whole blood (Damhorst et al. 2015; Curtis et al. 2016, 2012; Kemleu et al. 2016). The detection of Zika virus is confounded by the short window of detection of the virus in serum, urine, and saliva (Fourcade et al. 2016; Gourinat et al. 2015; Musso et al. 2015). However, two independent reports have suggested detectable amounts of Zika viremia in whole blood for up to 2 months (Lustig et al. 2016a), and 81 days (Murray et al. 2017) after the onset of symptoms and attributed this prolonged Zika viremia presence to the erythrocyte component of whole blood. Several other studies on West Nile and Dengue viruses have reported similar findings showing a large proportion of viruses bound to red blood cells leading to 10-fold higher concentrations and much longer persistence of viruses in whole blood compared to plasma (Lai et al. 2012; Lanteri et al. 2014; Rios et al. 2007; Lustig et al. 2016b; Klungthong et al. 2007). These findings suggest whole blood is likely the ideal body fluid for diagnosis as well as long-term viral load monitoring in Zika infection. To date there have been no point-of-care assays reported which include this erythrocyte-associated component with minimal sample processing (Song et al. 2016; Pardee et al. 2016). Additionally, none of the previously published literature on LAMP-based Zika diagnostics have answered the critical concern of multiplexing multiple closely related viruses on a single platform.

Herein, we report an integrated, lab-on-a-chip method for detection of Zika virus in spiked whole human blood employing complete hands-free sample processing, a unique RT-LAMP assay, and smartphone imaging. Our assay is quantitative and can detect down to 10 PFU/reaction which corresponds to 1.56e5 PFU/mL of Zika virus in infected blood in under 35 min with minimal sample processing. To further extend the clinical significance of our work, we multiplex the detection of Zika virus with RNA from other closely related viruses- Dengue virus types 1 and 3, and Chikungunya virus on a single microchip. We demonstrate the only platform to date that can multiplex detection of viral and other nucleic acid targets on a portable point-of-care setup starting from whole blood samples.

2 Methods

2.1 RT-LAMP reaction composition

All RT-LAMP assays comprised of the following components: 1× final concentration of the isothermal amplification buffer (New England Biolabs), 1.4 mmol/L each of deoxyribonucleoside triphosphates (dNTPs), 10 mmol/L of MgSO4 (New England Biolabs), and 0.4 mol/L of Betaine (Sigma-Aldrich). These components were prepared in bulk and stored at −20 °C between experiments. In addition to the buffer components, 3 μL of primer mix consisting of 0.2 μM of F3 and B3, 1.6 μM FIP and BIP, and 0.8 μM of LoopF and LoopB, 0.64 U/μL Bst 2.0 WarmStart DNA Polymerase (New England Biolabs), 0.08 U/μL AMV reverse transcriptase (New England Biolabs), and 1× EvaGreen (Biotium), a double-stranded DNA (dsDNA) intercalating dye, was included in the reaction. 8 μL template of the appropriate concentration and 0.05 μL of DEPC-treated water (Invitrogen) was added to make the final reaction volume 25 μL.

The RT-PCR reaction was carried with iTaq™ Universal One-Step RT-qPCR Kit (Bio-Rad Technologies). Briefly, a 20 μL final reaction mix contained 10 μL of 2× iTaq universal probes reaction mix, 0.5 μL of iScript advanced reverse transcriptase, 2 μL of 0.4 μM forward primer, 2 μL of 0.4 μM reverse primer,2.8 μL of 0.2 μM probe, and 2.7 μL of template RNA.

The templates for the Zika virus RT-LAMP characterization consisted of either purified RNA in water, or whole virus particles spiked in whole blood. Ten-fold serial dilutions of the templates in appropriate buffer were amplified to determine the working range of our developed assays. The RT-PCR reactions were performed with purified RNA in water. For the multiplexing tests (Fig. 3 & 6), the templates for Dengue-1, Dengue-3, and Chikungunya virus consisted of the corresponding viral RNA spiked in whole blood and the Zika virus template consisted of whole Zika virus spiked in whole blood. The off-chip co-infection test included an amalgam of purified viral RNA in water such that the final concentration of each target was 1000 PFU/reaction. All the off-chip and on-chip RT-LAMP and RT-PCR reactions consisted of non-template negative controls that were included in all the datasets. In the on-chip experiments, these non-template negative controls on-chip were prepared off-chip and injected into the appropriate lanes manually using a syringe. Additionally, the on-chip tests also included no primer negative controls to check for any cross-talk between adjacent wells.

2.2 Reaction platforms

All the off-chip LAMP tests were carried out in 0.2 mL PCR reaction tubes in an Eppendorf Mastercycler® realplex Real-Time PCR System. The tubes were incubated at 65 °C for 50 min in the thermocycler, and fluorescence data was recorded every 1 min. The off-chip PCR tests were conducted on the same thermocycler but with the following recipe: RT incubation at 50 °C for 10 min, 3 min of DNA denaturation at 95 °C, and 45 cycles of thermocycling from 95 °C (15 s) to 60 °C (60 s). Fluorescence data was recorded after each cycle of the reaction. All the on-chip experiments were carried out on a silicon biochip using our integrated point-of-care imaging and heating setup as described below.

2.3 Sample processing module

The microfluidic sample processing module was adapted from the work of Watkins et al. (Watkins et al. 2013) Polydimethylsiloxane (PDMS) was synthesized and poured over a SU-8 master mold fabricated using standard cleanroom photolithography techniques. The PDMS was then degassed in a vacuum desiccator and incubated in a 60 C oven for 2–3 h to cure. Cured PDMS block of thickness approximately 5 mm was then cut out from the mold and cleaned with Isopropyl Alcohol (IPA) followed by drying with dry nitrogen to remove any impurities from the microfluidic channels. Three inlet holes and one outlet hole were drilled into the PDMS using a 0.5 mm needle, for tubing connections. Afterwards, the surfaces of the processed PDMS and a clean glass slide were activated via oxygen plasma activation in a DIENER PICO plasma system. Immediately following this, PDMS and glass slide were covalently bonded to each other over a hot plate at 120 °C to form the complete sample processing module.

The sample processing module consisted of three inlet ports for three different solutions- whole Zika virus or other viral RNA spiked whole blood, RT-LAMP reagents and lysis buffer. The flow rates were controlled using syringe pumps, and were fixed at 1 μL/min, 3 μL/min, and 10.62 μL/min for virus/RNA in whole blood, lysis buffer, and RT-LAMP reagents respectively. This setup was kept in the biosafety cabinet, and biosafety level 2 protocols were followed during these experiments.

2.4 Amplification chip fabrication

The oxidized silicon chip was roughly the size of a quarter (29 mm × 29 mm) and has 6 interconnected channels at the center and 2 separate, independent channels along the periphery. Flow channel dimensions were 10 mm in length, 500 μm in width and 200 μm in depth, representing a volume of 1 μL per channel. The inlet of the chip was a 2 mm diameter circle. A 4-in. <100> silicon wafer (University Wafer, South Boston, MA) with one side polished was thoroughly cleaned and used as the substrate in the photolithography process. Positive photoresist SPR 220 (MicroChem, Newton, MA) was spin-coated on the polished side of the wafer to form a 4.5 μm covering layer, followed by the soft-bake at 60 °C for 2 min and 110 °C for 1 min. The photoresist was then exposed with an i-line (365 nm) mask aligner (EVG 620) with an expose dose of 180 J/cm^2. The exposed regions with the outline of the microfluidic pattern were subsequently removed by immersing the wafer in AZ developer diluted 1:4 with deionized (DI) water for 4 min. The photoresist in the unexposed regions was solidified though a hard-bake at 110 °C for 1 min. For the anisotropic etching of the silicon substrate, a Bosch process RIE with alternating steps of SF_6/O_2 etching and C_4F_8 passivation was used to create a 200 μm deep trench. After the Bosch process, the remaining photoresist was stripped with acetone and O_2 plasma cleaning, leaving the bare silicon exposed. Finally, the wafer was thermally oxidized in a furnace (1150 °C) for 2 h to grow 200 nm SiO_2 and subsequently scribed into individual chips.

2.5 Cradle fabrication and smartphone based fluorescence imaging

The optical imaging system used to excite and detect fluorescent emission from the LAMP assay is depicted in Fig. 1. The system is composed of a smartphone (Nexus 6; Motorola, IL, USA) and a portable 3D–printed cradle that supports the optical and electrical components and interfaces with the rear-facing camera (13 megapixels, pixel size of 1.4 μm) of the smartphone. Not only does the cradle align the camera with the components, but it serves as a dark chamber for pure

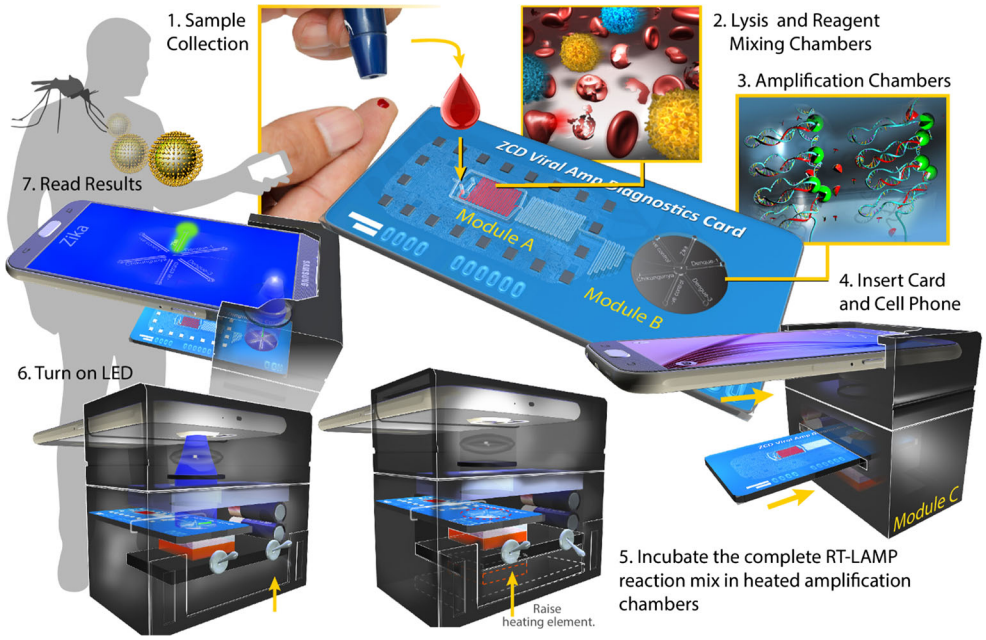

Fig. 1 Schematic and POC process flow of the ZCD Viral Detection system. 1. Patient sample form a finger prick of blood is collected and loaded into the pre-processing module. 2. Automated on-chip mixing of the sample with the lysis buffer and RT-LAMP reagents takes place within minutes in sample processing module (module A). 3. The complete reaction mix is loaded onto the amplification chip (module B). 4. The amplification module is completely sealed and ZCD Viral Diagnostics Card is inserted into the cradle. 5. The smartphone is positioned on top of the cradle and focused to image the entire chip. The heating switch is turned on to incubate the amplification chip for the RT-LAMP reaction. The silicon amplification chip sits atop the heating element and is in contact with the heater during the entire RT-LAMP incubation process. 6. The LED switch is turned on for sample illumination. 7. Real-time fluorescence imaging of the amplification reaction is performed using the smartphone and the results of the RT-LAMP reaction are visually displayed on the smartphone screen. The lighting up of a channel indicated the presence of the corresponding pathogen in the patient blood

fluorescence detection by blocking out external light. The smartphone paired with the cradle takes photos of the chip at 1-min intervals to and communicates with a cloud-connected external computing system to process image data.

A schematic of the system is shown in **Fig. S7b**. The top part of the cradle holds the smartphone and allows the rear-facing camera to align with an opening that supports a macro lens (12.5X) and a long pass filter (525 nm). The macro lens is placed in front of the camera to enable close-up photography of the chip, which reduces the distance between the camera and the chip to 50 mm, while keeping the 29 X 29 mm chip within the field of view. The long pass filter allows only light generated by the assay fluorophores to be transmitted to the camera. A light-emitting diode (LED) module composed of eight SMD type blue LEDs (λ_{peak} = 485 nm, $V_{forward}$ = 3.1 V) and four short pass filters (490 nm) that cover each pair of LEDs is installed in the cradle to excite fluorescence of the EvaGreen intercalating dye. The LEDs are mounted on a printed circuit board (PCB) and arranged with square symmetry to provide uniform illumination over the microfluidic chip area. The light source module is powered and operated by an Arduino Gemma, which is an open-source electronics platform composed of a programmable circuit board and control software. The Arduino microcontroller board is powered by a lithium-ion battery (3.7 V) and provides 3.3 V output by a built-in voltage regulator that powers all eight LEDs consistently. The preprogrammed Arduino board regulates the duty cycle and operation frequency of the LED On-Off switching during a measurement. For experiments with viral RNA in water, the LED "on" time was 6.1 s, and the "off" time was 53.9 s, and for experiments of RNA/whole virus particles in whole blood, the LED "on" time was set to 10 s, and the "off"time was set to be 50 s. The card that contains the amplification chip is inserted into the cradle such that it is in contact with the positive temperature coefficient (PTC) heater that allows the chip temperature to stabilize near 65 C without an external temperature controller. The PTC heater is made from a ceramic material that functions as a self-regulating heating element, such that when the temperature of the PTC heating element increases, the electrical resistance increases nonlinearly resulting in decreased heat output to set the temperature at a predesigned limit. The PTC heater does not require an over-temperature protector, while providing uniform heating, low-voltage operation, and light weight. The PTC heater (12 V-80 °C; Uxcell, Hong Kong, China) is powered by a battery set (10.5 V) composed of two standard 9 V batteries and two 1.5 VAA batteries each to set the temperature of the microfluidic chip around 66 ~ 68 C for 60 min to perform one LAMP assay (**Fig. S8**). The LEDs and the heater are turned on and off by two separate toggle switches. The

transmitted fluorescent light through the macro lens and long pass filter is captured using the smartphone rear-facing camera in an 8-bit 3-channel JPG image format. The overall dimensions of the system are ~90 X 70 X 95 mm^3.

2.6 Amplification chip preparation, chip assembly, and chip sealing

All the microfluidic chips for on-chip RT-LAMP experiments were cleaned in the following steps: First, the chip was cleaned in a Piranha solution containing 1:3 of 30% hydrogen peroxide and sulfuric acid for 10 min followed by extensive rinsing with deionized water to remove any acidic residues. Then, the chip was dried using nitrogen gas and immersed in Sigmacote (Sigma-Aldrich) in a sterile petri dish for approximately 5 min to make the surface of the chip and its channels hydrophobic. This was done to prevent any non-specific adsorption of biomolecules on the chip surface during the RT-LAMP reactions (Duarte et al. 2013). The chip was then rinsed with isopropanol before being blow-dried with nitrogen gas. Chips were placed in sterile glass petri dishes until use.

Primers were printed on the positive and non-template negative reaction channels followed by a short incubation period at room temperature to dry the primers. Briefly, 1× concentration of the primer was diluted in 1:3 ratios in DEPC treated water and two drops of 0.24 μL of primers were pipetted and left to dry at room temperature for 30 min. Following drying, double sided adhesive membranes (ARSeal 90,880, Adhesive Research), each with 11 laser-cut holes attached to three small PDMS blocks with holes drilled by a 0.5 mm needle was aligned and attached to the microfluidic silicon chips. PDMS blocks were aligned with three inlet ports on the chip- a central inlet port for sample injection, and two peripheral inlet ports for injection of non-template negative controls. The assembled chips were stored in a desiccator until use.

For experiments with viral nucleic acids in water, the template and the RT-LAMP reagents were mixed off-chip, and then injected into the chip using a syringe pump. Once the sample was loaded into the chip, the outer layer of the double-sided adhesive which contained the PDMS blocks was peeled off, and the chip was sealed with a second double-sided adhesive layer to prevent evaporation during RT-LAMP incubation. The chip was placed on a credit card sized cartridge (85.6 mm × 54.0 mm × 0.8 mm), and the cartridge containing the amplification chip was inserted into our portable point-of-care setup for RT-LAMP reaction, and real-time monitoring. The cartridge fit snugly inside the cradle which ensured good contact with the heater throughout the LAMP incubation step.

For any experiments involving blood, the sample processing chip and the amplification chip were assembled together on the cartridge (Fig. 1). A tube from the outlet of the pre-processing chip connected the sample injection port of the amplification chip ensuring rapid, reliable, and automated mixing and sample loading into the amplification chip. The amplification chip was visually observed for filling, and the connecting tube was manually disconnected once filling was complete. The chip was sealed in the same procedure as described above. The cartridge containing both the sample pre-processing chip and the amplification chip was inserted into the cradle. The amplification chip rested atop the heater inside the cradle while pre-processing chip stuck out. Biosafety level-2 protocol was observed in all experiments with live viruses.

2.7 Image and data analysis

Images recorded with IP Webcam in smartphones were saved in TIFF format from which fluorescence intensity was analyzed in an automated fashion using a MATLAB script. Grayscale images were first imported as an array of 8-bit unsigned integers (range 0–255), which represented each pixel in the image. Then, the average fluorescence intensity from only the channel portions of the chip were extracted using a polygonal virtual mask. Such time-lapsed fluorescence values for each channel were obtained from the images and a fluorescence vs time curve was plotted. The baseline (initial) fluorescence value was subtracted for each curve to account for the differences in starting fluorescence values per channel. The fluorescence measurements in the data were in arbitrary units (AU).

All on-chip and off-chip RT-LAMP and RT-PCR data was analyzed and plotted using a MATLAB script. For all the off-chip and on-chip experiments, the threshold time was taken as the time taken for an amplification curve to reach 20% of its maximum intensity. For on-chip reactions, the fluorescent intensity on-chip was extracted from each channel and was plotted against time to generate the raw fluorescence curves. Each raw amplification curve was fitted to a sigmoidal curve using a four-point parameter modeling (Fig. S6). The following equation was used for the analysis:

$$f = y_0 + \frac{a}{1 + e^{-\left(\frac{x - x_0}{b}\right)}}$$

Where f = fluorescence intensity, y_0 = background fluorescence at time = 0 min, a = difference between the initial and final fluorescent intensity, x = time point of analysis, x_0 = inflection point of the curve, b = slope of the curve. The threshold time was obtained at the point where the fluorescent intensity = $y_0 + 0.2^{*}a$. The positive and negative wells were differentiated based on the R^2 value of the sigmoidal fit and the parameters a and x_0. Negative wells had a combination of low R^2 value, low a value, or a very high threshold time (x_0>50 mins).

3 Results and discussion

3.1 Overview of approach

Fig. 1 shows the process flow for our on-chip multiplexed pathogen detection from a finger prick of whole blood sample. Our point-of-care diagnostics and monitoring platform can be divided into three primary modules: A, B and C. Module A is a polydimethylsiloxane (PDMS) microfluidic sample processing chip where infected whole blood is first lysed and then mixed with amplification reagents. This chip has three inlets ports for infected blood, lysing buffer and RT-LAMP amplification reagents respectively, and one outlet port for amplification-ready processed analyte. The robustness of RT-LAMP reaction to inhibitors allows for replacing the usual RNA purification steps required before amplification reactions with simple cell lysis and our on-chip sample processing module A translates the routine manual pipetting steps to a complete hands-off platform. Next, the processed sample from Module A is transferred to Module B, which is an oxidized silicon chip with six etched micro-channels (1 cm X 500 μm X 200 μm), for isothermal amplification at 65C. RT-LAMP primers specific to different pathogens are predried in different channels of the chip as a part of chip preparation. After the processed sample is transferred into these channels, the chip is sealed with a silicone based adhesive (ARseal™ 90,880, Adhesives Research) to prevent sample evaporation during incubation. As shown in Fig. 1, the modules A and B are incorporated in a "diagnostics card" which is similar to a credit card in appearance and this card can be customized according to the pathogens to be detected or quantified in the patient blood by pre-printing the specific primers. Module C is our point-of-care setup comprising of a commercial smartphone, an in-built heater and the essential optics/optical accessories for real-time fluorescence imaging. The details about this setup are discussed in the experimental section. Once the "diagnostics card" and the smartphone are in place, the heater and the blue LED for sample illumination are turned on and real-time fluorescence imaging of the on-chip RT-LAMP reaction is performed using the smartphone. The reaction mix contains a double-stranded DNA intercalating dye which yields fluorescence as the reaction progresses. Only the channel with primers specific to the pathogen in patient blood sample lights up over time whereas the fluorescence for the other channels remains at an initial baseline level. Amplification curves are generated with this real-time fluorescence data and threshold times for amplification are obtained. Pathogen concentration can be inferred from these threshold times using a standard curve. This quantitative capability of our platform becomes crucial in scenarios where changes in pathogen concentration in patient samples need to be monitored over time, such as for viral load monitoring in response to retroviral therapy in HIV patients (Yager et al. 2008), and in Dengue virus infections where high viremia presentation has been linked to secondary infection and disease severity (Waggoner et al. 2016b).

3.2 Characterization of RT-LAMP in a benchtop thermocycler

As a first step towards our goal, we designed a novel RT-LAMP reaction for Zika virus RNA. Six sequence specific primers for the NS1 gene of PRVABC59 Zika virus strain (Genbank: KU501215) were designed (Supplementary Note 2). Zika virus PRVABC59 was isolated from the blood of a human in Puerto Rico in December 2015 (Lanciotti et al. 2016). NS1 gene in Zika virus has previously been used for specifically detecting Zika virus using RT-PCR assay (Waggoner and Pinsky 2016). Fig. 2 shows the off-chip characterization of our RT-LAMP assay in a standard benchtop thermocycler apparatus. Zika virus RNA was purified by the Qiagen Viral Purification Kit. Fig. 2a-b show the baseline-subtracted change in fluorescent intensity over time for different concentrations of Zika virus RNA, and the corresponding threshold time against the PFU (plaque forming units)per reaction. We observed a good linear fit for the standard curve ($R^2 = 0.9755$) and a lower limit of detection of 10 PFU equivalent of purified RNA per reaction (reaction volume = 25 μL) corresponding to 1250 PFU/mL purified RNA in starting concentration. To compare our Zika virus RT-LAMP reaction with the previously published CDC RT-PCR assay for Zika virus (Lanciotti et al. 2008), we carried out RT-PCR experiments with same Zika virus RNA concentrations as used for RT-LAMP using the CDC RT-PCR primers and obtained the amplification and standard curves. Fig. 2c-d show the baseline-subtracted change in fluorescent intensity over time for different concentrations and the corresponding standard curve for the RT-PCR assay, respectively. The lower limit of detection for the RT-PCR assay was found to be 1 PFU equivalent of purified RNA per reaction (20 μL) corresponding to 370 PFU/mL purified RNA in starting concentration. A similar novel RT-LAMP reaction was designed and characterized for the MR 766 (Rhesus/1947/Uganda) strain of the Zika virus (Genbank: AY632535.2) and compared to CDC RT-PCR assay as shown in Fig. S1 and S2. A good linear fit was observed for the standard curve ($R^2 = 0.9755$), and the lower limit of detection was determined to be 10 PFU equivalent of purified RNA per reaction which corresponded 1250 PFU/mL purified RNA starting concentration.

As a next step, to characterize the feasibility of our developed RT-LAMP reaction from minimally processed samples, different concentrations of whole Zika virus were spiked in lysed whole blood and the reactions were performed in a thermocycler. Fig. 2e-f show the baseline-subtracted change in fluorescent intensity over time for different concentrations of viruses and the corresponding threshold time against whole

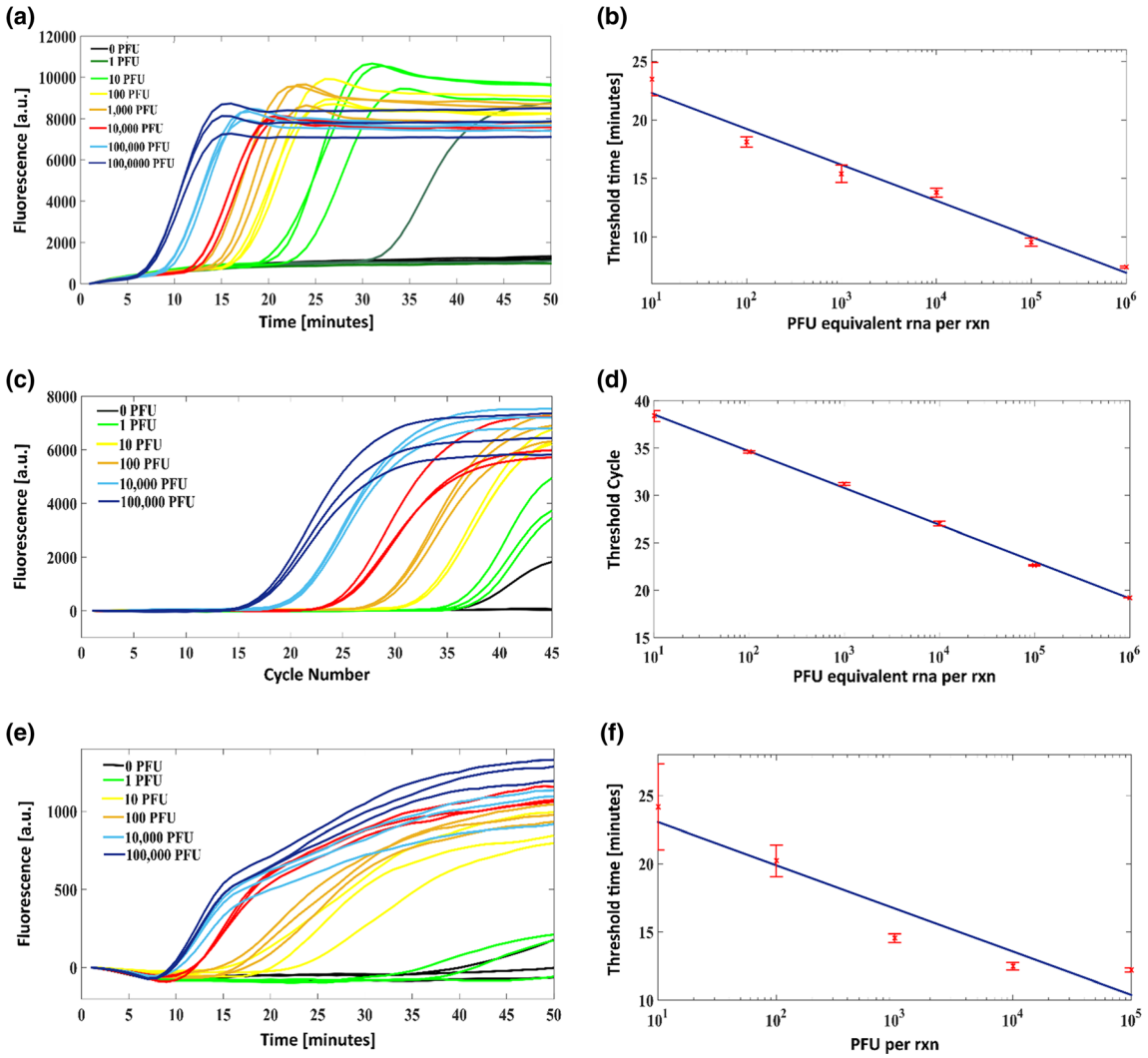

Fig. 2 Thermocycler based Zika virus RT-LAMP reaction characterization. **(a-b)** Baseline-subtracted raw amplification curves showing the change in fluorescence over time and the calculated standard curve of the RT-LAMP assay for Zika virus PRVABC59 purified RNA. **(c-d)** Baseline-subtracted raw amplification curves showing the change in fluorescence over time and the standard curve of the RT-PCR assay for Zika virus PRVABC59 purified RNA. This assay was performed using previously published primers (Lanciotti et al. 2008). **(e-f)** Baseline-subtracted raw amplification curves showing the change in fluorescence over time and the standard curve of the RT-LAMP assay for whole Zika virus PRVABC59 spiked in lysed whole blood. The results demonstrate the range and lower limit of detection of our assay in thermocycler based reactions from purified Zika virus RNA and whole Zika virus in lysed whole blood

Zika virus PFU per reaction. Similar to the RT-LAMP reaction with purified RNA, Zika virus spiked in lysed whole blood showed a good linear fit for the standard curve ($R^2 = 0.9047$) and a lower limit of detection of 10 PFU per reaction in 25 μL tube based reactions. This corresponded to a starting Zika virus sample concentration of 6250 PFU/mL in blood. We observed reduced fluorescence intensity in RT-LAMP reactions with lysed whole blood which is consistent with previous reports (Damhorst et al. 2015). These results show that our RT-LAMP reaction is robust to the debris present in lysed whole blood and serve as a proof-of-concept for our on-chip reactions from processed whole blood.

As our final goal was to perform multiplexed pathogen detection on the same chip, we selected two other closely related viruses – Dengue virus (types 1 and 3) and Chikungunya virus to multiplex with Zika virus on our chip. Since Zika virus infection shares symptoms with other febrile diseases such as Dengue and Chikungunya, accurate diagnosis is required to differentiate these infections during the acute phase of the disease. As RT-LAMP reactions for these pathogens already existed in literature (Hu et al. 2015; Parida et al. 2007, 2004), we used these previously published primers (Supplementary Note 2) and validated them in a tube-based thermocycler reaction. Fig. S4 shows the amplification curves for Dengue-1, Dengue-3, and Chikungunya RNA in water as a test of previously published primers. Fig. 3 shows the amplification curves for the RT-LAMP reactions from Dengue-1, Dengue-3, Chikungunya virus, and Zika virus RNA spiked in

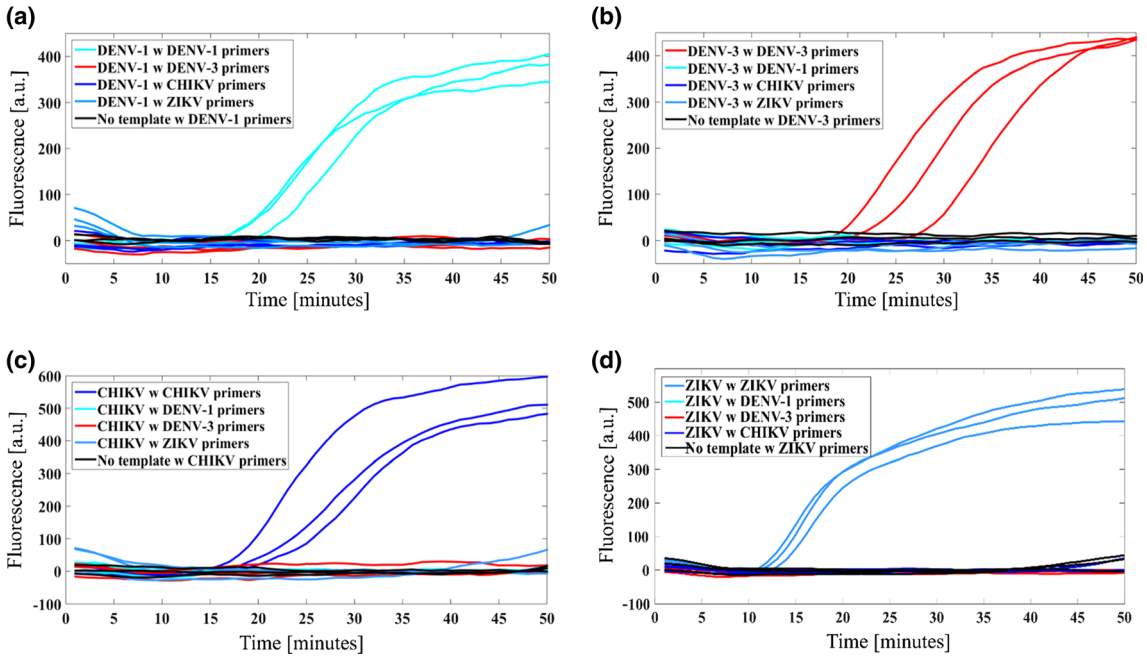

Fig. 3 Off-chip multiplexing of four viral targets. Baseline-subtracted raw amplification curves showing the changes in fluorescence over time in separate RT-LAMP reactions to detect **(a)** Zika virus **(b)** Dengue-1 virus **(c)** Dengue-3 virus, and **(d)** Chikungunya-virus templates. All the templates were challenged with all the primer sets and the result demonstrates that only the correct template-primer pair amplifies. The template in Fig.s a-c contain 1000copies/reaction (25 μL volume) of Dengue-1, Dengue-3 and Chikungunya purified RNA spiked in lysed whole blood. The template in Fig. d contains 1000PFU/reaction (vol = 25 μL) of whole Zika virus spiked in lysed whole blood

lysed whole blood against different primer sets. As summarized in Supplementary Table 1, only the specific template-primer pairs amplify in each of the panels validating the usability of these primer sets in multiplexing experiments. We also demonstrate the specificity of our Zika virus assay in the rare case of co-infection where multiple pathogens might be present simultaneously in the patient blood sample. As shown in Fig. S3, we demonstrate in a tube-based thermocycler reaction that our assay can specifically detect Zika virus in the presence of Dengue-1, Dengue-3, and Chikungunya virus simultaneously in a single reaction.

3.3 Microfluidic chip based sample processing

The next step towards a complete point-of-care system was to process the infected blood sample on-chip to make it suitable for amplification. In a two-step process, the infected whole blood was first mixed with lysing buffer and then with amplification reagents in a PDMS microfluidic chip. Fig. 4c shows the complete process flow and the chip layout, and Fig. S7**a** shows images of the integrated chip. Independent characterization of this microfluidic sample processing module was done to compare its performance with routine manual pipetting/mixing based methods and to assess its potential for automation and integration with our point-of-care setup. 10 μL of whole blood sample spiked with 625 PFU/ μL Zika virus was metered and injected into the PDMS microfluidic chip concurrently with lysis buffer and RT-LAMP reagents through the labelled inlets. The output was collected from this microfluidic chip on four separate instances and RT-LAMP experiments on each instance were performed on a thermocycler. As a control, four replicates of the same Zika virus spiked whole blood sample were mixed with lysis buffer and RT-LAMP reagents manually using a pipette and analyzed in a thermocycler. Fig. 4a shows the amplification curve for the two mixing scenarios, and Fig. 4b shows the corresponding threshold time bar graphs. The threshold times for on-chip and manual sample processing technique were found to very similar with the deviation in the on-chip processing threshold time being 3.6% from the off-chip processing threshold time. The on-chip mixing was also confirmed visually by observing different regions of the chip during the processing step and Fig. 4c shows the bright-field microscopy images of these regions.

3.4 Characterization of micro-chip Zika virus RT-LAMP assay

After the characterization of the RT-LAMP reactions in a thermocycler, we translated and characterized these reactions on our microchip and performed them on our novel point-of-care setup. RT-LAMP reactions with purified Zika virus RNA in water and Zika virus spiked in whole blood were performed on our microchip with ten-fold serial dilutions and the working range and limit of detection of our assays were determined. The integrated heater in our setup maintained temperature 66–68 C, which was appropriate for our reactions. Fig. S8 shows the results for our point-of-care setup heater characterization. Real-

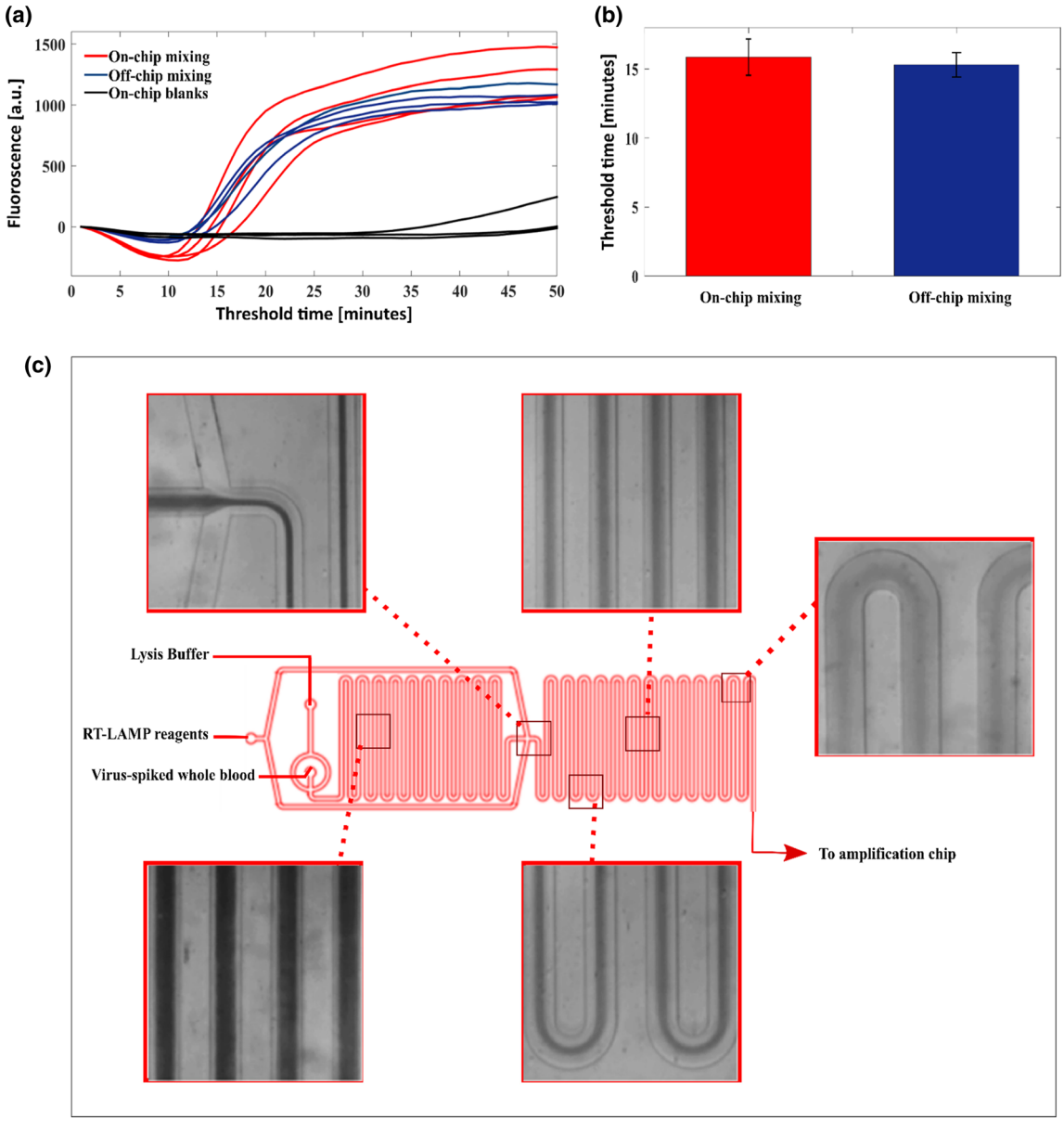

Fig. 4 Microfluidic sample processing characterization. **(a)** Baseline-subtracted raw amplification curves showing the changes in fluorescence over time for on-chip and off-chip sample processing (blood lysis and reagent mixing) using whole blood sample containing 625 PFU/μL Zika virus. **(b)** Threshold-time bar graphs comparing the on-chip and off-chip sample processing. The final product of the microfluidic mixing was pipetted into tubes and thermocycler based RT-LAMP reactions were performed. Control thermocycler based RT-LAMP reactions with same Zika virus in blood concentrations were performed after sample processing through manual pipetting. **(c)** Images showing mixing of the blood-lysis buffer- amplification reagents at different points in the channels of the sample processing chip

time images were captured by smartphone and threshold time analysis was performed using a MATLAB script, details about which are mentioned in the experimental and supplementary sections. For both sets of experiments, three alternating channels (in the primary hexagon shape) on the microchip, and two separate non-template negative control channels on the chip periphery were printed with Zika virus primers. The remaining three channels are left unprinted to serve as on-chip no-primer controls which are simultaneously performed in each experimental run. Thus, our chip in total has three positive reaction channels, three negative no-primer control channels and two negative no-template control channels as shown in the chip layout (Fig. 5). Together they ensure that the amplification results obtained are from specific Zika virus reactions only and not from spurious, non-specific amplification.

For the on-chip RT-LAMP characterization with purified RNA, template (purified RNA in water) and the RT-LAMP reagents without primers were mixed manually using a pipette, and 7 μL of the final reaction mix was injected into the amplification chip (module B) using a syringe pump. The chip was sealed to prevent evaporation (See Supplementary section for details) and contamination, and the diagnostics card consisting

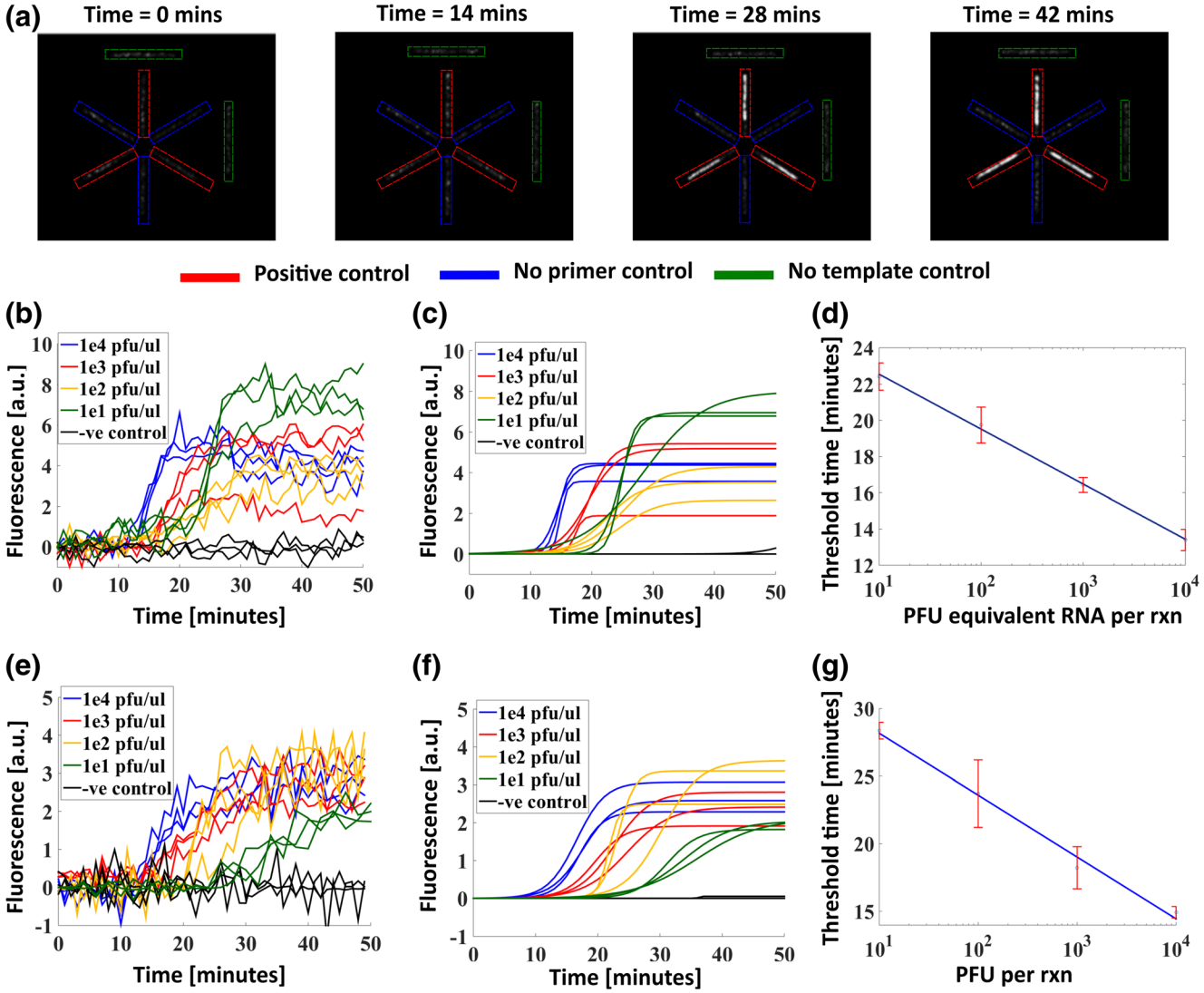

Fig. 5 On-chip RT-LAMP assay characterization. **(a)** Raw fluorescence images of the amplification chip at time = 0, 14, 28, and 42 mins respectively showing the amplification of only positive channels for RT-LAMP reaction with purified RNA. The images shown are for 1e1 PFU equivalent of purified RNA/μL of Zika virus in final reaction. **(b)** Raw amplification curves of the Zika virus RT-LAMP assay on-chip carried out from purified RNA, and **(c)** the same amplification curves after sigmoidal fitting. **(d)** The standard curve of the Zika virus RT-LAMP assay with purified RNA. A lower limit of detection of 3.125e4 PFU equivalent of purified RNA /mL in starting sample of Zika virus RNA in water was observed. **(e)** Raw amplification curve of the Zika virus RT-LAMP assay on-chip carried out with whole viruses in whole blood and **(f)** the same amplification curves after sigmoidal fitting. **(g)** The standard curve of the Zika virus RT-LAMP assay with virus in whole blood. A lower limit of detection of 1.56e5 PFU per mL of Zika virus in starting infected blood sample was observed. All experiments involving blood were carried out using the integrated setup

the amplification chip was inserted into the cradle. Fig. 5a shows the time-lapsed fluorescence images of a representative RT-LAMP reaction on-chip showing the amplification of only positive channels. The images shown are for RT-LAMP reaction from 10 PFU equivalent of purified RNA per microliter of Zika virus. Fig. 5b-d show the raw amplification curves, the amplification curves after sigmoidal fitting, and the threshold-time standard curves for these reactions. The details about sigmoidal fitting analysis are mentioned in the experimental section and illustrated in Fig. S6. We observe a lower limit of detection of purified RNA equivalent to 10 PFU per μL of final reaction (1 channel = 1 reaction = 1 μL volume) corresponding to 3.125e4PFU/ mL in starting concentration). A good linear fit was observed in the standard curve (R^2 = 0.99) with distinct threshold times per ten-fold change in template concentration.

The complete diagnostics card with the sample processing chip (module A) connected to the amplification chip (module B) as shown in Fig. 1b, was used to characterize the RT-LAMP reactions with Zika virus in whole blood. The Zika virus infected blood sample was first processed in module A as described in the previous section and then allowed to flow directly into the amplification chip. Upon filling, the chip was sealed, and the diagnostics card was inserted into the cradle (point-of-care setup). The cradle design allows the

amplification chip to sit snugly on top of the heater while the sample processing module sticks out as shown in Fig. S7a. Fig. 5e-g show the raw amplification curves, the amplification curves after sigmoidal fitting, and the threshold-time standard curves for these reactions A good linear fit was observed in the standard curve (R^2 = 0.9913) with Zika virus detection down to 10 copies per μL of final reaction (1 channel = 1 reaction = 1 μL volume) corresponding to 1.56e5 PFU/ mL starting virus concentration. With clinically significant detection limits from infected blood samples, the results of this experiment demonstrated that our on-chip assay can successfully monitor viral loads via RT-LAMP reactions that employs hands-free sample processing, a portable cradle setup, and smartphone-based imaging that can be easily translated for use at the point-of-care.

3.5 Multiplexed pathogen detection on microchip

Our platform was put to the final test of analyzing samples containing different pathogens on the diagnostics card. Zika

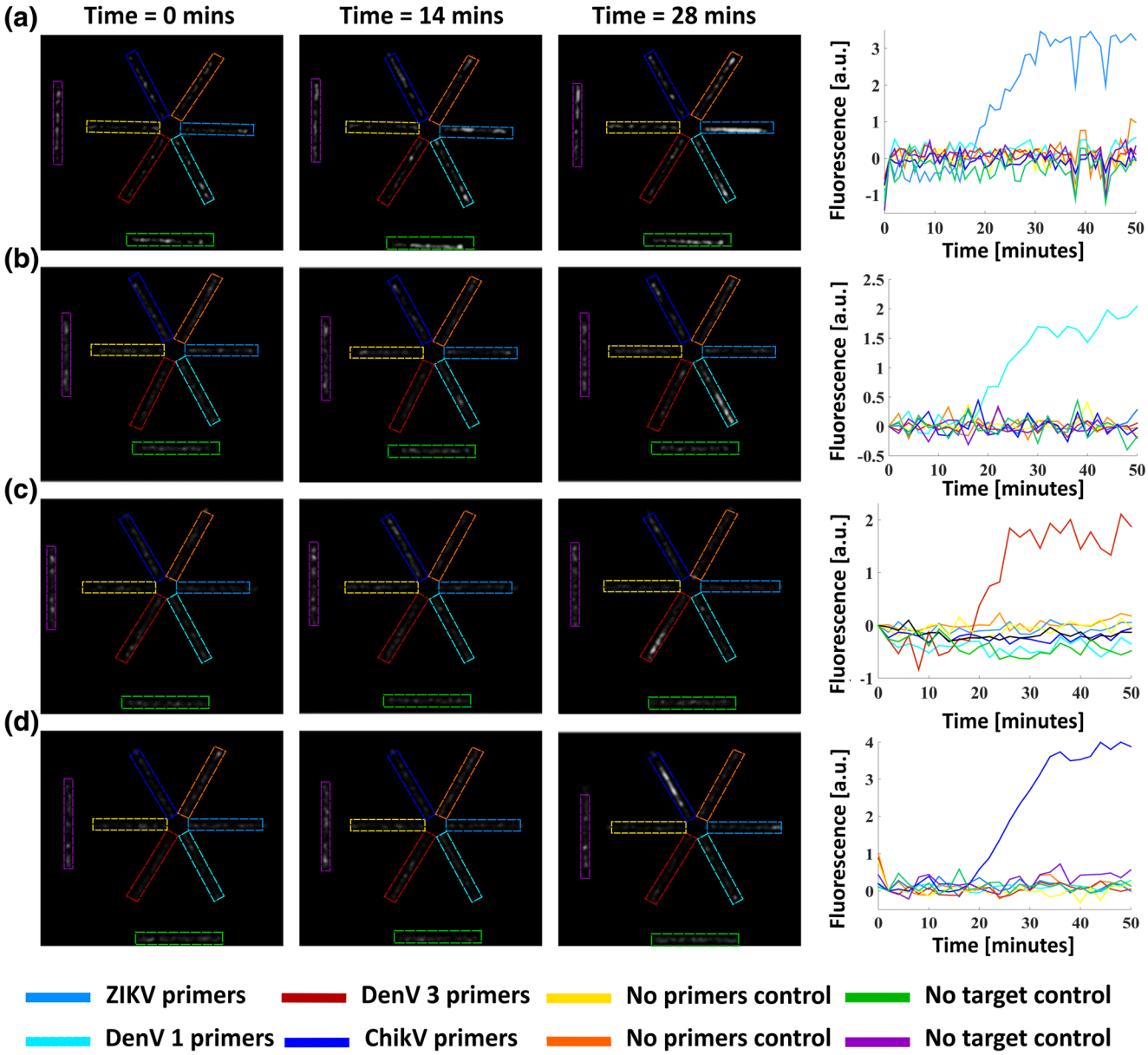

Fig. 6| On-chip multiplexing of four viral targets. Raw fluorescence images of the amplification chip at t = 0, 14, and 28 min respectively and raw amplification curves of the RT-LAMP reaction showing multiplexed detection of **(a)** Zika virus **(b)** Dengue-1 viral RNA **(c)** Dengue-3 viral RNA, and **(d)** Chikungunya viral RNA from infected whole blood samples in four separate experiments using the same chip layout with pre-printed primers. Primers for each of these pathogens were simultaneously printed in different channels of the chip and this layout was kept constant across the different on-chip multiplexing experiments. The starting concentration of Zika virus and the other viral RNAs in blood was equal to 1.56e4 PFU or copies/μL in starting blood sample

virus, Dengue-1, Dengue-3, and Chikungunya virus primers were simultaneously printed in different channels on our amplification chip (module B) per the pattern shown in Fig. 6. The complete integrated setup was used for these experiments to demonstrate their efficacy in a clinical setting. The chips were challenged with either 1.56e4 PFU/μL of whole Zika virus in starting blood sample or 1.56e4 copies/μL of purified RNA of either Dengue-1, Dengue-3, or Chikungunya virus in starting blood sample and separate point-of-care RT-LAMP experiments were performed. Fig. 6a-d show the multiplexed detection of Zika virus, Dengue-1, Dengue-3, and Chikungunya virus from whole blood respectively. In each of the case, we observe that only the lanes with specific template-primer set amplify while the remaining lanes remain at baseline fluorescence during the entire reaction. These reactions demonstrate the capability of our platform to specifically diagnose and provide clinically actionable information for different pathogens at the point-of-care from infected whole blood samples.

4 Conclusions

Among the barriers to more effective management of Zika virus outbreaks, such as the recent episode in South and Central America, is the lack of an adequate tools for diagnosis. Neither clinical presentation nor serology testing can reliably distinguish Zika from other mosquito-borne viruses like Dengue and Chikungunya, yet early identification of Zika infection is critical to minimizing human-to-human transmission and preventing potentially devastating sequelae, such as fetal microcephaly (Kleber de Oliveira et al. 2016). Recent reports have included higher viral loads and much longer persistence of viruses detectable in whole blood compared to plasma, urine, and other biological samples. However, none of the point-of-care approaches on Zika infection detection to date have tapped into the erythrocyte-associated viral load component. Enabling regular detection of these viruses in whole blood may allow for new, clinically-relevant information not available in assays which only assess plasma or serum viral load. For example, this could elucidate relationships between detectable erythrocyte-associated virus fraction and transmission potential of an infected individual. We have demonstrated detection of Zika virus as low as 1.56e5 PFU/mL from whole blood with a microchip and smartphone-based point-of-care platform. While reports are varied, the viral loads in only the serum component of whole blood have been documented as high as 1e6 PFU/mL (Faye et al. 2008), and hence, we believe our technique is capable of addressing the clinically-relevant range when testing from whole blood samples. This makes our work one of the most compelling approaches yet to be reported toward making available a practical tool for Zika diagnostics due to its rapid performance, portable format, and ability to distinguish Zika from related infections. Furthermore, we expect limit-of-detection can be further improved in subsequent iterations of this technology to meet the need to detect even very low viremia at the point-of-care.

Furthermore, our approach is capable of quantitative analysis of viral load which is likely to prove valuable in the understanding of a previously little-known pathogen. For example, one report has associated high viremia with hospitalization and increased severity of symptoms (Waggoner et al. 2016b), so a quantitative measure of viral load may prove valuable in triage or guidance of anticipatory management of individuals with confirmed infection. Meanwhile, another report identified very high viremia in a case in which non-sexual, close-contact transmission took place (Swaminathan et al. 2016), suggesting that the ability to quantitate viral loads may inform the need for contact precautions or quarantine (Waggoner et al. 2016b). Low reagent consumption and the ability to test for multiple pathogens on a single pre-printed microchip is the basis for our platform's potential to achieve low-cost testing from a simple finger prick. The process is compatible with freeze-drying methods which would enable single-use, disposable biochips to be prepared and stored before rehydrating in a re-usable system. Our battery-powered 3-D printed cradle with an embedded optical detection system and integrated heater, coupled with smartphone imaging also lends itself to portable and user-friendly operation with low instrument costs. The smartphone gives real-time visual output of the test which can be interfaced directly with an external computer or completely self-contained with data analysis performed by a mobile application. The clear integration with mobile communications technology allows personalized patient care and facilitates information management for both healthcare providers and epidemiological surveillance efforts. Finally, while we have demonstrated the multiplexing of Zika, Dengue type 1, Dengue type 3 and Chikungunya viruses from whole blood, our platform exhibits the flexibility to incorporate alternative or additional targets simply by preparing the appropriate primer sequences on the printed microchip.

Acknowledgements We thank the staff at the Micro and Nanotechnology Laboratory at UIUC for facilitating the chip fabrication. The work was funded by NSF grant 1534126 and the University of Illinois at Urbana-Champaign.

Author's Contributions A.G., A.O., G.L.D, B.T.C and R.B conceived the idea and designed the study. A.G. and A.O., designed and performed the experiments. G.L.D and A.B assisted with the experiments and provided intellectual inputs. H.Y. developed the cradle interface for the smartphone and performed the setup characterization experiments. W.C. and F.S developed the fabrication process for the microfluidic chip. A.G developed image processing algorithms to derive fluorescence intensity values from the assay lanes of the microfluidic chip. All wrote and edited the manuscript.

Compliance with ethical standards

Competing interests The authors declare no competing financial interests.

References

L.R. Baden, L.R. Petersen, D.J. Jamieson, A.M. Powers, M.A. Honein, N. Engl. J. Med. **374**, 1552–1563 (2016)

K. Curtis, D. Rudolph, I. Nejad, J. Singleton, PLoS One (2012)

K.A. Curtis, D.L. Rudolph, D. Morrison, D. Guelig, S. Diesburg, D. McAdams, R.A. Burton, P. LaBarre, M. Owen, J. Virol, Methods **237**, 132–137 (2016)

G.L. Damhorst, C. Duarte-Guevara, W. Chen, T. Ghonge, B.T. Cunningham, R. Bashir, Eng. **1**, 324–335 (2015)

C. Duarte, E. Salm, B. Dorvel, B. Reddy, R. Bashir, Biomed. Microdevices **15**, 821–830 (2013)

C. Duarte-Guevara, F.-L. Lai, C.-W. Cheng, B. Reddy, E. Salm, V. Swaminathan, Y.-K. Tsui, H.C. Tuan, A. Kalnitsky, Y.-S. Liu, R. Bashir, Anal. Chem. **86**, 8359–8367 (2014)

C. Duarte-Guevara, V.V. Swaminathan, B. Reddy, J.-C. Huang, Y.-S. Liu, R. Bashir, RSC Adv. **6**, 103872–103887 (2016)

O. Faye, O. Faye, A. Dupressoir, M. Weidmann, M. Ndiaye, A. Alpha. **43**, 96–101 (2008)

C. Fourcade, J. Mansuy, M. Dutertre, M. Delpech, B. Marchou, P. Delobel, J. Izopet, G. Martin-blondel, J. Clin. Virol. **82**, 1–4 (2016)

A. Gourinat, O. O. Connor, E. Calvez, C. Goarant, Emerg. Infect. Dis. **21**, 84–86 (2015)

S. Hu, M. Li, L. Zhong, S. Lu, Z. Liu, J. Pu, J. Wen, BMC Mol. Biol. 1–15 (2015)

S. Kemleu, D. Guelig, C. Eboumbou Moukoko, E. Essangui, S. Diesburg, A. Mouliom, B. Melingui, J. Manga, C. Donkeu, A. Epote, G. Texier, P. LaBarre, R. Burton, L. Ayong, PLoS One **11**, e0165506 (2016)

W. Kleber de Oliveira, J. Cortez-Escalante, W.T.G.H. De Oliveira, G.M.I. do Carmo, C.M.P. Henriques, G.E. Coelho, G.V. Araújo de França, MMWR Morb. Mortal. Wkly Rep. **65**, 242–247 (2016)

C. Klungthong, R.V. Gibbons, B. Thaisomboonsuk, A. Nisalak, S. Kalayanarooj, V. Thirawuth, N. Nutkumhang, M.P. Mammen, R.G. Jarman, J. Clin. Microbiol. **45**, 2480–2485 (2007)

L. Lai, T.H. Lee, L. Tobler, L. Wen, P. Shi, J. Alexander, H. Ewing, M. Busch, Transf. **52**, 447–454 (2012)

R. S. Lanciotti, O. L. Kosoy, J. J. Laven, J. O. Velez, A. J. Lambert, A. J. Johnson, S. M. Stan, M. R. Duffy, 14 (2008)

R. S. Lanciotti, A. J. Lambert, M. Holodniy, S. Saavedra, C. Castillo, Emerg. Infect. Dis. **22**, 2015–2017 (2016)

M.C. Lanteri, T.H. Lee, L. Wen, Z. Kaidarova, M.D. Bravo, N.E. Kiely, H.T. Kamel, L.H. Tobler, P.J. Norris, M.P. Busch, Transfusion **54**, 3232–3241 (2014)

D. Lee, Y. Shin, S. Chung, K. S. Hwang, D. S. Yoon, J. H. Lee, Anal. Chem. **88**(24), 12272–12278 (2016). doi:10.1021/doiacs.analchem.6b03460

J. Lessler, L. H. Chaisson, L. M. Kucirka, Q. Bi, K. Grantz, H. Salje, A. C. Carcelen, C. T. Ott, J. S. Sheffield, N. M. Ferguson, D. A. T. Cummings, C. J. E. Metcalf, I. Rodriguez-Barraquer, Sci. **46**(80), 601–604 (2016)

V. van der Linden, A. Pessoa, W. Dobyns, A.J. Barkovich, H. van der L. Júnior, E.L.R. Filho, E.M. Ribeiro, M. de C. Leal, P.P. de A. Coimbra, M. de F. V. V. Aragão, I. Verçosa, C. Ventura, R.C. Ramos, D.D.C.S. Cruz, M.T. Cordeiro, V.M.R. Mota, M. Dott, C. Hillard, C.A. Moore, MMWR Morb. Mortal. Wkly Rep. **65**, 1343–1348 (2016)

Y. Lustig, E. Mendelson, N. Paran, S. Melamed, E. Schwartz, 1–4 (2016a)

Y. Lustig, B. Mannasse, R. Koren, S. Katz-likvornik, **54**, 1–16 (2016b)

K. O. Murray, R. Gorchakov, A. R. Carlson, R. Berry, L. Lai, M. Natrajan, M. N. Garcia, A. Correa, S. M. Patel, K. Aagaard, M. J. Mulligan, Emerg. Infect. Dis. **23**, 99–101 (2017)

D. Musso, C. Roche, T.-X. Nhan, E. Robin, A. Teissier, V.-M. Cao-Lormeau, *Detection of Zika virus in saliva*, **68**, (2015)

T. Notomi, H. Okayama, H. Masubuchi, T. Yonekawa, K. Watanabe, N. Amino, T. Hase, **28**, (2000)

T. Notomi, Y. Mori, N. Tomita, H. Kanda, J. Microbiol. **53**, 1–5 (2015)

K. Pardee, A.A. Green, M.K. Takahashi, D. Braff, G. Lambert, J.W. Lee, T. Ferrante, D. Ma, N. Donghia, M. Fan, N.M. Daringer, I. Bosch, D.M. Dudley, D.H. O'Connor, L. Gehrke, J.J. Collins, Cell **165**, 1255–1266 (2016)

M. Parida, G. Posadas, S. Inoue, F. Hasebe, K. Morita, **42**, 257–263 (2004)

M. M. Parida, S. R. Santhosh, P. K. Dash, N. K. Tripathi, V. Lakshmi, N. Mamidi, A. Shrivastva, N. Gupta, P. Saxena, J. P. Babu, P. V. L. Rao, J. Clin. Microbiol. **45**, 351–357 (2007)

M. Rios, S. Daniel, C. Chancey, I.K. Hewlett, S.L. Stramer, Clin. Infect. Dis. **45**, 181–186 (2007)

M. Safavieh, M. K. Kanakasabapathy, F. Tarlan, M. uddin Ahmed, M. Zourob, W. Asghar, H. Shafiee, ACS Biomater. Sci. Eng. (2016). doi:10.1021/acsbiomaterials.5b00449

J. Song, M.G. Mauk, B.A. Hackett, S. Cherry, H.H. Bau, C. Liu, Anal. Chem. **88**, 7289–7294 (2016)

S. Swaminathan, R. Schlaberg, J. Lewis, K. E. Hanson, M. R. Couturier, 1907–1909 (2016)

B. Tian, Z. Qiu, J. Ma, T. Zardán Gómez de la Torre, C. Johansson, P. Svedlindh, M. Strömberg, Biosens. Bioelectron. **86**, 420–425 (2016)

J. J. Waggoner, A. Pinsky, J. Clin. Microbiol. **54**, 860–867 (2016)

J. J. Waggoner, L. Gresh, A. Mohamed-hadley, G. Ballesteros, M. Jose, V. Davila, Y. Tellez, M. K. Sahoo, A. Balmaseda, E. Harris, B. A. Pinsky, **22** (2016a)

J.J. Waggoner, L. Gresh, M.J. Vargas, G. Ballesteros, Y. Tellez, K.J. Soda, M.K. Sahoo, A. Nuñez, A. Balmaseda, E. Harris, B.A. Pinsky, Clin. Infect. Dis. **63**, 1–7 (2016b)

X. Wang, F. Yin, Y. Bi, G. Cheng, J. Li, L. Hou, Y. Li, B. Yang, W. Liu, L. Yang, J. Virol, Methods **238**, 86–93 (2016)

N. N. Watkins, U. Hassan, G. Damhorst, H. Ni, A. Vaid, W. Rodriguez, R. Bashir, Sci. Transl. Med. (2013). doi:10.1126/scitranslmed.3006870

P. Yager, G.J. Domingo, J. Gerdes, Annu. Rev. Biomed. Eng. **10**, 107–144 (2008)